Wear under brittle removal regime of an under-expanded cryogenic nitrogen jet machining of bio-composites

Floriane Lavorel [a,c], Mohamed El Mansori [a,b], Faissal Chegdani [a,*], Abdel Tazibt [c]

[a] Arts et Métiers Institute of Technology, MSMP, HESAM Université, F-51006, Châlons-en-Champagne, France
[b] Texas A&M Engineering Experiment Station, Institute for Manufacturing Systems, College Station, TX77843, USA
[c] CRITT TJFU, Laboratoire Jets Fluides Complexes Impactants & Matériaux, 55000, Bar-le-Duc, France

ARTICLE INFO

Keywords:
Abrasive jet cutting
Impact
Surface topography
Polymer-matrix composite

ABSTRACT

Machining of biocomposites using traditional techniques has shown some limitations due to the multiscale complex cellulosic structure of natural fibrous reinforcement. This paper aims to demonstrate the feasibility of the cryogenic nitrogen jet, which is a novel cutting process that combines sustainable resources and cryogenic temperatures from −175 °C to 150 °C, as a machining process for biocomposites made of unidirectional flax fibers and polylactic-acid polymer (PLA). A high-velocity stream of liquid nitrogen with and without abrasives (400–700 m/s) is hence directed onto the workpiece surface. For the abrasive jet, both conventional garnet abrasives and bio-based abrasives made from walnut shells were used for the nitrogen jet process. The kerf depth, which is representative of the erosion wear mechanisms, was calculated to assess the erosion rate of the biocomposite structure after the nitrogen jet cutting operation. Then, scanning electron microscope observations are performed to characterize the induced damages on the machined biocomposite surfaces. Results show that the pressure and the traverse speed of the nitrogen jet are the relevant process parameters that control the mechanical and thermal stresses viewed by the biocomposite during the machining operation. Each impinging abrasive particle removes a small amount of biocomposite material during the jet cutting process, which depends on the brittleness of the anisotropic work structure and the abrasiveness of the incorporated particles into the jet stream.

1. Introduction

Natural fiber reinforced composites (so-called biocomposites to denote fiber-reinforced polymer composite materials where the fibers and/or matrix are bio-based) have captured the industry's attention as they are low cost and have very high specific characteristics [1]. This type of ecofriendly polymer composites has been studied over the past decades to substitute synthetic glass fiber composites. Fiber reinforced polymer composites are considered as hard-to-machine materials because of the high contrast of mechanical properties between the different components [2]. Indeed, the mechanical properties of fibers are largely higher than that of polymer matrices. These latter are either brittle for thermosets or ductile for thermoplastics [3]. In this work, the polylactic-acid (PLA) matrix (mostly hydrophobic) reinforced with flax fibers (highly hydrophilic) is considered as a 100% bio-based composite that has good mechanical properties [4]. Flax fibers are well-known as a complex multiscale structure: an elementary fiber is made by the association of three different cell walls constituted mainly of cellulose and hemicelluloses held by lignin, pectin, and waxy compounds [5], as described in Fig. 1(a) and (b). This structure allows the fiber to follow a visco-elastoplastic behavior under mechanical loading. The non-linear behavior of flax fibers was attributed to the rearrangement of cellulose microfibrils toward the fiber axis [6].

PLA is a polymer made from natural polysaccharides which are highly biodegradable [4]. It can be amorphous or semi-crystalline depending on the chirality of its molecules. Many researchers studied phase transitions of polymer and composite materials. For PLA, its chirality gives stereoisomers with a wide range of melting point between 130 °C and 230 °C. Below the melting point, two more phase transitions can be noticed for stereoisomers: around 58 °C for the glass transition and −45 °C for the β transition (ductile to brittle temperature transition i.e. DBTT) [8]. PLA, as well as flax fibers, have low thermal conductivity (λ_{PLA} = 0.110–0.195W/m.K [9], λ_{flax} = 0.040 W/mK [10]). Scientific and industrial interests for PLA were revealed from 2000, and mainly for

* Corresponding author.
E-mail address: faissal.chegdani@ensam.eu (F. Chegdani).

3D printing or film applications [11], limiting hence the literature investigation on its behavior under 0 °C.

On the other side, few literature works have investigated the thermal properties of natural fibers and natural fiber composites. Sanadi et al. [12] have studied the transition temperatures of kenaf/polypropylene (PP) biocomposites to show the trans-crystallinity at the interfaces. An α-relaxation temperature, corresponding to the presence of defects within the amorphous phase, was found at 70–80 °C. Moreover, a β transition around 0 °C was found to be similar to the PP glass transition temperature (−20 °C) increased from the interactions of the matrix with the cellulose, lignin and oils [12]. Back et al. [13] showed that moisture impacts the glass transition temperature of wood components such as cellulose, hemicellulose (from around 230 °C in its dried state to −10 °C at 30% of water content), and lignin (from 200 °C to 0 °C with less than 10% water content). It has been shown that flax fibers contain around 10% of water content [14], which can impact significantly the composite's phase transition temperature.

Traditional machining of composites such as drilling and orthogonal cutting creates numerous defects within a composite material such as delamination, fuzzing, fraying, and deformation in heat-affected zones [15]. Different types of wear occur during a machining operation: adhesion wear, abrasive wear, impact wear, and friction [16]. The heterogeneity of composite materials leads to complicate their machinability, especially for biocomposites because the weak interfaces between natural fibers and the polymer matrix may create microdefects inside of the composite. Le Duigou et al. [17] investigated the interface between flax fibers and an epoxy matrix, showing that it is a complex interface mixing chemical and physical adhesion. Orthogonal cutting of biocomposites has shown that the flexural properties of natural fibers limit the machined surface's quality by favoring deformation, bending, and pull-out of elementary fibers [18]. Moreover, the multiscale tribo-mechanical behavior of flax fibers, including nano-adhesion and nano-friction mechanisms between the cellulosic components [19], could also contribute to the complex machining behavior of bio-composite structures. Wang et al. [20] explored the effect of ultrasonic-assisted drilling on bio-composites. The energy needed to cut the fibers is lowered by the ultrasonic waves, which reduces the damages induced by the machining. Chegdani et al. [21] showed that lowering the sample temperature improves the machined surface of flax fiber composites by reducing the machining-induced temperature seen by the material, thus preventing the fibers' deformation. Indeed, the shearing of flax fibers is not efficient at room temperature because of excessive transverse deformation as shown in Fig. 2(a) where the cross-section shapes of flax fibers are not obvious on the microscopic observation. By lowering the sample temperature before machining, the fiber shearing is improved and the cross-section of flax fibers are more distinguished with their lumen in the middle as shown in Fig. 2(b).

To prevent the heat-affected zone (HAZ), researchers have sought out other techniques such as water jet machining [22] and cryogenic-assisted machining [23] to keep the material's surface from deteriorating under the high tribo-mechanical machining stresses. Accordingly, lowering the temperature of a material enhances its rigidity, hence strengthening the chemical bonds to find the equilibrium of the lowest energy [24]. Morkavuk et al. [25] have used liquid nitrogen (LN_2) instead of the usual coolants on carbon fiber reinforced composites before and during the machining operation. Their experiments showed that cryogenic machining reduces the surface damages as well as the delamination within the material although the cutting forces were increased. Cryogenic pre-treatment also seemed to enhance the mechanical properties of the composites.

To lower a material's temperature, different thermal exchange mechanisms can be used such as conduction, convection, and radiation [26]. When using a high-pressured fluid, the main thermal exchange is done through forced convection. Equation (1) defines the heat transfer per unit of time ϕ where h is the heat transfer coefficient, A is the surface exposed to the jet, T is the temperature of the material, T_f is the temperature of the nitrogen jet, and b is an exponent.

$$\phi = Ah(T_f - T)^b \tag{1}$$

It can be concluded that biocomposite machining has been emphasized until today in studying and searching for cutting conditions to avoid the induced thermo-mechanical damages using known conventional or non-conventional cutting processes. In this paper, a cryogenic fluid extracted from a renewable nitrogen resource is used as an under-expanded cryogenic nitrogen jet (UCNJ). The UCNJ will be applied to the machining of flax fiber reinforced PLA composites as a substitute to the conventional machining processes. In this renewable and sustainable machining process, a cryogenic regenerative tool is considered instead of the conventional cutting tools used in traditional cutting processes. From previous experiments, the UCNJ is expected to behave as the water jet process [27].

Water jet represents the most understood fluid jet machining. Soft (polymers) and hard-to-machine materials (composites/metals) can be machined respectively with pure or abrasive water jets [28]. The high-pressure water jet gains velocity when it passes through a small nozzle's orifice. Equation (2) gives the speed of the fluid jet after the nozzle (v_{fj}), where p is the static pressure of the nitrogen jet, ρ_f is the density of the fluid, and k is a discharge coefficient of the nozzle [29] (k~0.8).

$$v_{fj} = k\sqrt{\frac{2p}{\rho_f}} \tag{2}$$

When using a pure water jet, the energy of the fluid (E_{fj}) can be calculated from Equation (3) using the fluid mass m_{fj}, and its velocity v_{fj} which is equivalent to using the fluid mass flow rate q_{fj} and the exposure time t_e. Water jet can also be characterized by its fluid jet power P_{jf} that depends on the nitrogen's static pressure p and the fluid mass flow rate q_{fj} following Equation (4).

$$E_{fj} = \frac{1}{2}m_{fj}v_{fj}^2 = \frac{1}{2}q_{fj}v_{fj}^2 t_e \tag{3}$$

$$P_{fj} = p \times q_{fj} \tag{4}$$

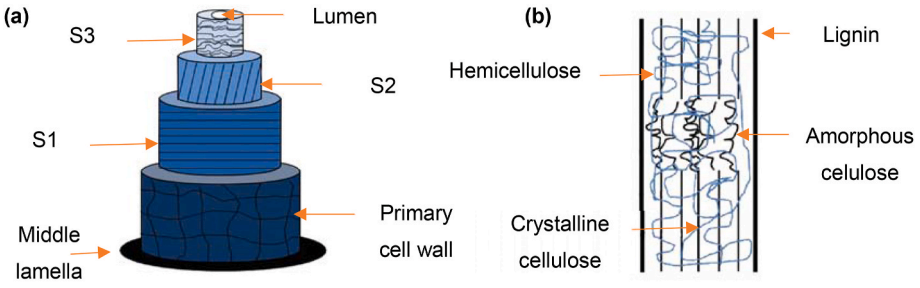

Fig. 1. Schematic depiction of (a) an elementary flax fiber showing the primary and the secondary (S1, S2, S3) cell walls (b) structure of the second cell wall made of amorphous and crystalline cellulose embedded in hemicellulose and enclosed by lignin [7].

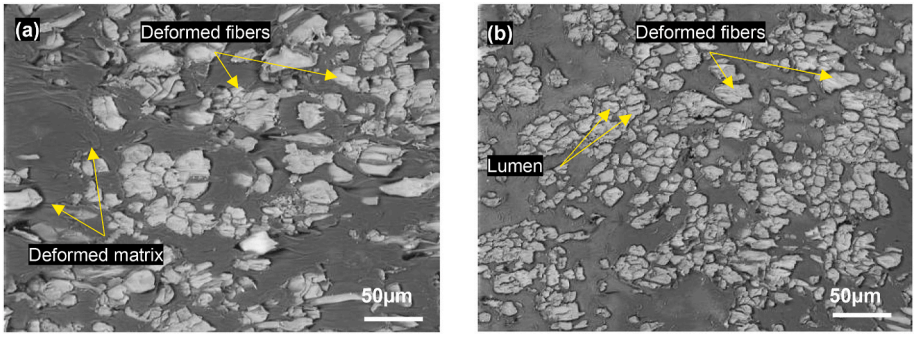

Fig. 2. SEM images of machined surfaces obtained by traditional orthogonal cutting of flax/PP composites at (a) room sample temperature (~22 °C), and (b) reduced sample temperature (~0 °C) using a cooling spray [21].

This kinetic energy is transferred to the abrasive particles within the mixing chamber and the mixing tube [30]. Equation (5) defines the energy accumulated by the abrasives E_{afj} and its dependence on the abrasive mass flow rate q, the nitrogen feed rate q_{fj}, the abrasive N_2 jet velocity v_{afj}, the N_2 jet speed v_{fj}, and the yield η [29]. The yield represents the loss of energy from the expansion of the N_2 fluid through the nozzle and its compressibility [31].

$$E_{afj} = \frac{1}{2} q v_{afj} = \frac{1}{2} q \eta^2 \frac{v_{fj}^2}{(1 + \frac{q}{q_{fj}})^2} \quad (5)$$

In a cutting operation, the fluid jet is orthogonal to the workpiece to maximize the impact wear on the surface and the abrasive wear from the particles once the tap is formed. This energized particle impacts the material, transferring a part of its energy to it, which creates a plastic deformation zone on the material beneath the particle and failures within the material. If the material is ductile, the energy will deform its surface as for a polymer at ambient temperature. However, if the material is brittle, the impact will form cracks on the surface leading to debonding and failure mechanisms which is the behavior of a polymer below its ductile to the brittle transition temperature. As the jet goes deeper into a sample, the fluid deviates when crossing the material's surface and thickness [32]. It follows the path of minimum resistance within the material as the jet loses its kinetic energy [33]. The abrasive particles are fragmented during the whole process from the mixing chamber to the sample machining. Ferrendier et al. [34] studied the impact of the granulometry of the abrasives on the fragmentation process. Many parameters, such as the pressure, the abrasive's nature, size, and granulometry were shown to have an impact on both the number of fragmentation steps and the final size of the particles. They also showed that increasing the sample thickness increases the fragmentation cycles.

The abrasive particles mostly used in industry for a similar process are garnet or silica sand [28]. Thus, garnet abrasive will be used in this investigation as a reference. To prevent sample pollution from metals and minerals, bio-based powders can be used as abrasives. For example, walnut shell powder, which is constituted of the same elements as flax fibers such as hemicellulose (22%), cellulose (25%), and lignin (52%) [35], is mostly used for sandblasting applications [36]. This material showed hydrophilic properties observed by FTIR analysis [37] as did flax fibers.

To avoid chemical reactions between PLA or flax fibers with the jet, especially the hydrolysis [38], the Nitrogen (N_2) jet, which is chemically inert, will be used herein as jet fluid. This substance is mostly used in cryogenic machining as a cooling lubricant to reduce the machining-induced temperature seen by the tool and the material [39]. Originally designed for the automatic cleaning of nuclear sites by Nitrocision [40], a high-pressure nitrogen jet has been used for coating removal [41] and surface texturing of metallic [42] and polymer materials [27]. The jet flow was studied by Dubs et al. [43], who modeled the evolution of the temperature and the pressure in the core of the jet. The temperature seen by the material will be considered in the range of −175 °C to −150 °C. Applying this process to the cutting of industrial materials needs better understanding.

From this literature review, some conclusions can be drawn. These include the following:

- Traditional machining techniques of biocomposites show technical limitations due to the complex structure of natural fibrous reinforcements;
- Transition temperatures such as glass temperature and DBTT (Ductile-Brittle Transition Temperature) influences the tribo-mechanical properties of the contact. These transition temperatures depend on the compositions of the fibers and the matrix;
- Using a regenerative cryogenic tool could improve the wear mechanisms by reducing the HAZ (heat-affected zone);
- The main parameters influencing fluid jet cutting are the fluid pressure, the abrasive nature, the abrasive properties, and the traverse speed

In this paper, two UCNJ techniques will be fundamentally studied to cut flax/PLA composites: pure nitrogen jet (Fig. 3 (a)) and abrasive nitrogen jet (Fig. 3 (b)).

The first method allows the understanding of the elementary erosion mechanisms depending on the jet pressure (from 100 MPa to 300 MPa) and temperature (from −175 °C to −150 °C). The second method incorporates abrasive particles into the nitrogen stream after the jet formation in the mixing chamber, which forms a triphasic jet that contains liquid nitrogen, abrasives, and air.

2. Materials and methods

Flax/PLA biocomposites were provided by "*Kairos Biocomposites – France*" as sheets of 300 × 300 × 3,5 mm^3. They were made by thermocompression of 11 layers of PLA films with 10 layers of unidirectional non-woven flax fabric at a temperature of 200 °C for 5 min and a pressure of 1 bar. The composite was then cooled from 200 °C to 25 °C in 7 min at 7 bars. Flax fabrics were provided by "*Ecotechnilin – France*" based on European linen harvests. The fiber volume fraction is estimated at 23.7% according to the volume density for flax fiber and PLA matrix is ρ_f = 1.4 g/cm^3 and ρ_m = 1.24 g/cm^3, respectively [44]. Flax/PLA samples for fluid jet machining are obtained by cutting the biocomposite sheets into straps of 300 × 30 × 35 mm (see Fig. 4) using a water jet with garnet abrasives.

The clamping system shown in Fig. 4 was designed as a high rigidity sample fixture for orthogonal UCNJ cutting to hold the biocomposite workpiece. The standoff distance between the workpiece and the jet is fixed at 3 mm to make the hypothesis that the pressure and temperature seen by the material with a pure nitrogen jet are the same as that of the liquid nitrogen jet. The gun is kept orthogonal to the biocomposite surface. In pure UCNJ, the first gun is the cutting tool for pure nitrogen

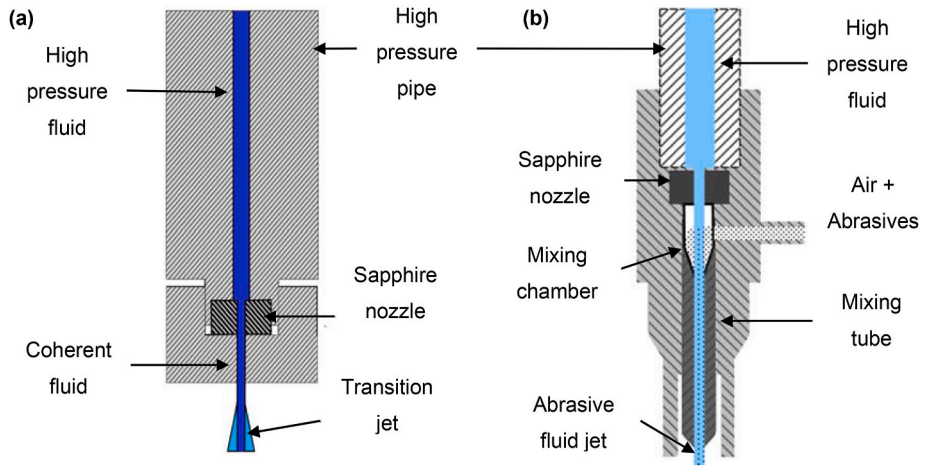

Fig. 3. A schematic of an under-expanded cryogenic nitrogen jet chamber. Mixing tube without abrasive (a), mixing chamber with abrasive nozzle (b).

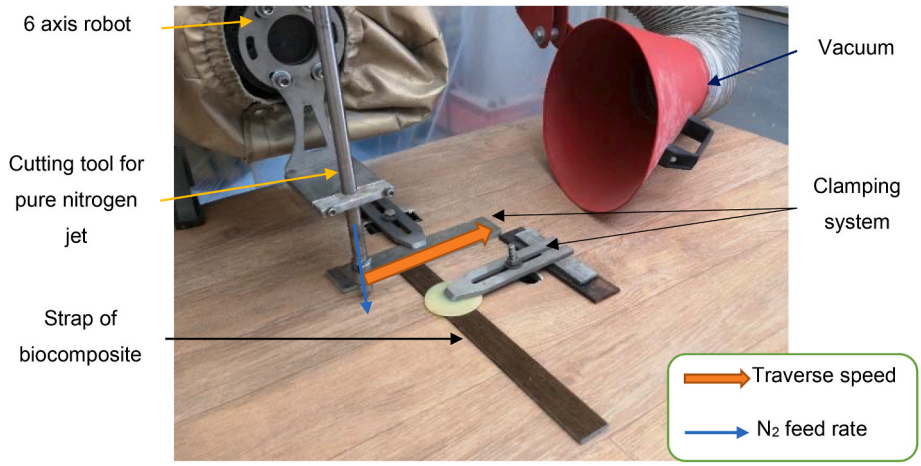

Fig. 4. Photography of the experimental set up for the pure nitrogen jet machining.

jet seen in Fig. 4 which can be depicted by Fig. 3 (a) and constituted of a sapphire nozzle of a 0.25 mm diameter. The second gun used is made for abrasive fluid jet as schematized in Fig. 3 (b) and is constituted of a sapphire nozzle of 0.30 mm, a mixing chamber, and a mixing tube defined by a length of 100 mm and an outlet diameter of 1.5 mm. Both garnet and bio-based walnut shell abrasive particles were used in this study with the same grit size of ~177 μm (i.e. 80 mesh). The properties of the considered abrasives are listed in Table 1 showing a representative microscopic surface of garnet and walnut shell grits.

To create the nitrogen jet, the NitroJet SKID designed by IHI-Nitrocision [27] was used as shown in Fig. 5. The liquid nitrogen is stored in a tank (1). It is drawn to a precooler (2) to maintain the liquid state and compressed into a pre-pump (up to 100 MPa - (3)). The compression heats the liquid into a supercritical state which will go back to the liquid state after another cooling. A second bench constituted of an intensifier (4), enables the fluid to be pressurized once again to a pressure of 300 MPa. Before reaching the gun, the fluid goes through a heat exchanger that stabilizes the cryogenic temperature within a range of −175 °C and −150 °C.

The LN_2 starts flowing at a security distance of 150 mm of the sample to ensure the right displacement speed of the gun during the operation (referred to as the traverse speed of the jet). A vacuum was used to evacuate the gaseous N_2 formed by the liquid N_2 expansion (1L of liquid nitrogen expands into 670L of gaseous nitrogen) as well as the composites' microchips.

The pressure range of the Nitrojet was explored from 100 to 300 MPa at the LN_2 inlet of the tool. The traverse speed has been investigated in the range of 50 – 4500 mm/min. The given temperatures correspond to the LN_2 temperature within the chiller. Table 2 summarizes all the process parameters of the UCNJ cutting process.

Table 1
Properties of the considered abrasives.

	Garnet	Vegetal
Composition	$SiO_2FeOAl_2O_3MgOCaOMnO$	Lignocellulosic materials extracted from walnut kernel
Hardness (Mohs)	7.5–8.0	3.5
Relative density (g/cm^3)	2.4	0.52–0.70
SEM image	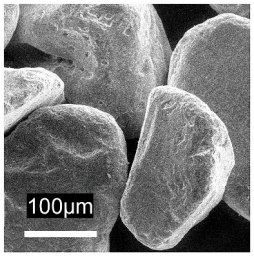 100 μm	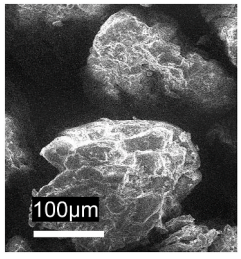 100 μm

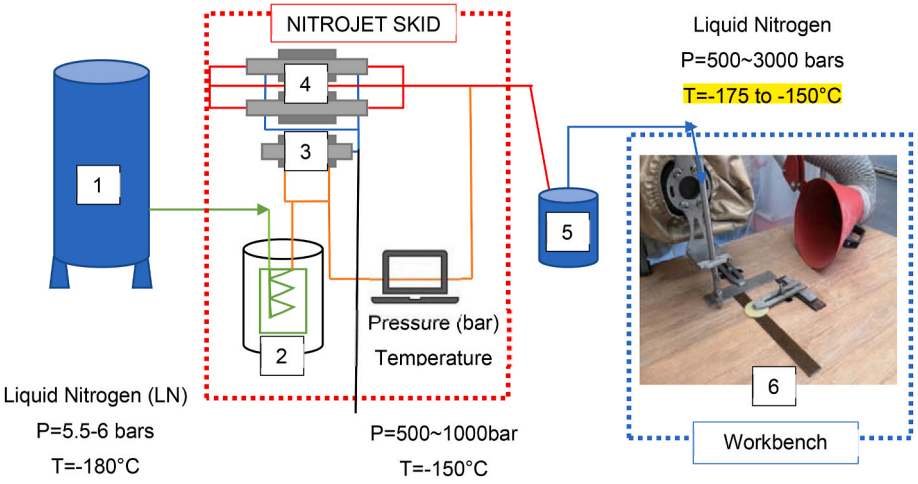

Fig. 5. Schematic depiction of the Nitrojet SKID machine composed of 4 main parts: (1) the storage, (2–4) the Nitrojet SKID to compress the liquid nitrogen, (2) a pre-cooler, (3) a pre-pump, (4) an intensifier, (5) a chiller ensuring the liquid state of the fluid, and (6) a workbench [27].

Table 2
Process parameters used for cutting flax/PLA biocomposites with under-expanded cryogenic nitrogen jet.

Process parameter	**Values and ranged used**
Pressure (P)	**100-200–300 MPa**
Jet temperature	−175 to −150 °C
Liquid Nitrogen feed rate	2L/s
Traverse speed of the N_2 jet (V_a)	50–4500 mm/min
Mixing tube length	100 mm
Mixing tube diameter	1.5 mm
Sapphire Nozzle diameter	0.25 mm for pure jet 0.3 mm for abrasive jet
Standoff distance	3 mm
Abrasives type	Mineral: Garnet Vegetal: Walnut
Abrasives granulometry	80 mesh
Abrasives mass flow rate (q_{garnet}) and (q_{walnut})	Garnet: 100–200–300 g/min Walnut shell: 65 & 165 g/min

Microscopic characterization of the machined surfaces was performed using a scanning electron microscope (SEM) (JSM-5510LV) at low vacuum mode (20–30 Pa of chamber pressure) to determine the cutting behavior of flax fibers and PLA matrix as well as the damages caused by the UCNJ machining. Typical representative SEM images of surface morphologies as induced by the UCNJ process were considered for each experimental configuration. Moreover, a stereomicroscope (SCHOTT – KL 1500) and the software Leica Application Suite (V 3.8.0) were used to estimate the erosion rate through the measure of the kerf depth.

3. Results

3.1. Pure nitrogen jet

For each couple of pressure/jet traverse speed parameters, the kerf depths were calculated to characterize the material loss induced by the nitrogen jet using Equation (6). Fig. 6 (a) shows a schematic of a single machined bio-composite workpiece with detail of calculation of the geometric characteristics, especially for uncut-through kerf viewed from the side, while Fig. 6 (c) shows the same schematic depiction viewed from above. For better visualization of the measurements, Fig. 6 (b) presents a photograph obtained by a Leica macroscope showing the same characteristics as previously described in Fig. 6 (a). The kerf depth was calculated in a normalized way to cancel the differences of height due to the composite's delamination using the following equation:

$$Kerf\ depth = \frac{sample's\ thickness - coherent\ material}{sample's\ thickness} \quad (6)$$

The delamination's thickness (Δh) can be seen in Fig. 6 (b) as well as its impact on the kerf depth measurement.

Fig. 7 (a) and (b) shows the logarithmic evolution of the erosion rate given by the normalized kerf depth variation during the orthogonal cutting by the UCNJ calculated for respectively the input and output of the workpiece. The depth of the jet penetration depends upon the pressure and the traverse speed of the jet. The uncut material was completely removed from the biocomposite at 300 MPa for a traverse speed of 3000 mm/min, and at 200 MPa for a traverse speed of 780 mm/min for the input of the jet – 50 mm/min for the output of the jet. However, under a pressure of 100 MPa, the jet was not energetic enough to cut through the 3.5 mm thickness of the material as can be seen in Fig. 7 (b). The depth of cut increases at high pressure and low traverse feed rate.

SEM observations were performed at machined surfaces that had an effective UCNJ cut (i.e. Kerf depth = 1). Therefore, the cutting configurations carried out with 100 MPa of jet pressure are not considered in the SEM analysis. Fig. 8 (a, b) presents SEM images of the surface features of a flax/PLA fiber reinforced polymer under a pure UCNJ cutting at 200 MPa. Chips of ~100 μm^2 were pulled out (BPC as brittle pulled-out chips in Fig. 8 (a, b)). Deformation zones (DZ in Fig. 9) can also be observed where fibers and matrix cannot be dissociated and present sharp edges. At 300 MPa (Fig. 8 (c, d)), the machined surface presents uncut fibers showing fibrillation. However, no signs of fiber pull out nor sharp edges are noticed.

However, a new detail appears at higher pressure and speed which is the presence of striations on the machined surface which seems to increase with the increase of the traverse speed showed in Fig. 9. To isolate the effect of the traverse speed (V_a), 3 machined surfaces with a constant pressure of P_{N2} = 300 MPa and V_a = {250; 500; 750} mm/min were analyzed using SEM micrographs as shown in Fig. 9. The density of uncut fibers and their lengths seems to increase with the increasing traverse speed.

3.2. Abrasive nitrogen jet cutting

Abrasive nitrogen jet was performed first using the well-known conventional garnet abrasive particles, and then the walnut shell abrasives, which are a new type of bio-based abrasive particles. Cutting tests are carried out for pressures of 100 and 200 MPa in a range of bio-composite traverse speed from 360 to 6000 mm/min to determine the

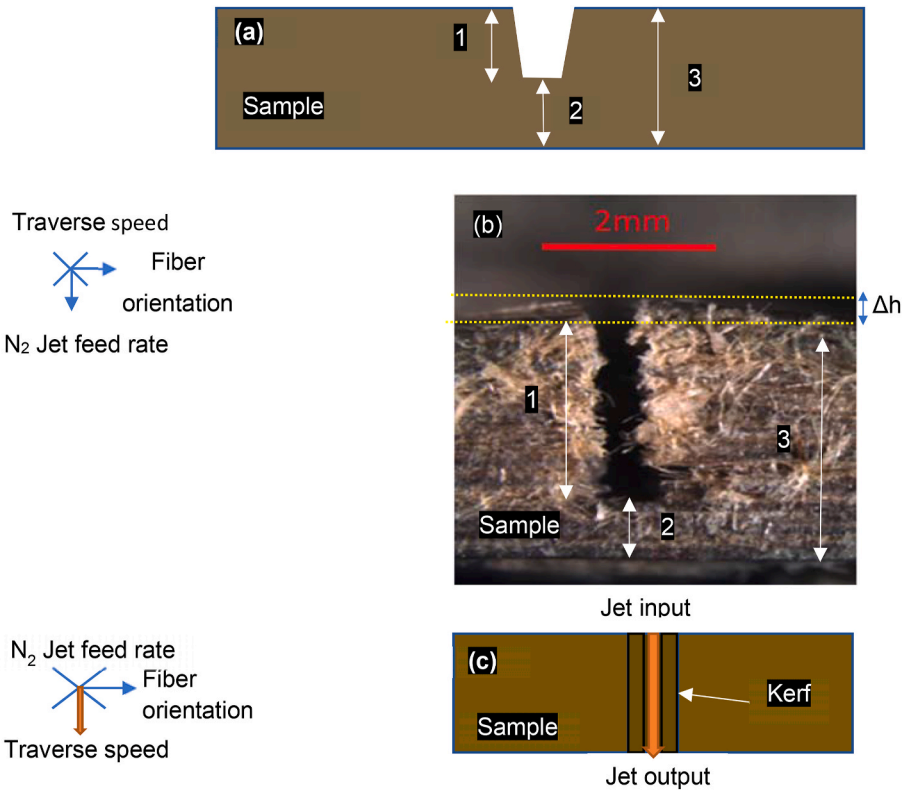

Fig. 6. (a) Representation of the kerf and the different measurements used in this study: (1) Kerf depth, (2) coherent material, (3) sample's thickness, (b) Optical observation of the kerf for a sample machined by a pure jet at (P = 300 MPa; V_t = 1000 mm/min) on which the coherent material's height (2) and the difference in height induced by the delamination from the machining (Δh) were measured, (c) Schematic depiction of the jet's input and output within the sample on the kerf depending on the traverse speed.

cutting capacities of the abrasives. Abrasives mass flow rate were respectively 65 and 165 g/min for the walnut shell, versus 100, 200, and 300 g/min for garnet. The material removal rate was determined using the kerf depth. Fig. 10 shows the erosion rate of the abrasive UCNJ using garnet at q_{garnet} = {100; 200; 300} g/min and walnut abrasives at q_{walnut} = 65 g/min and P_{NJ} = 100 MPa. From the graph Fig. 10, the abrasive mass flow rate does not show great influences on the erosion rate of the biocomposite and walnut abrasives seem less erosive as no cutting parameter was found for this type of abrasive material at 100 MPa.

In an attempt to determine the corresponding cutting parameters for the walnut abrasive, its mass flow rate was increased along with the pressure and showed, thus, an efficient cutting power only at low traverse speed (P_{N2} = 200 MPa; V_a = 360 mm/min) which is slightly higher than the pure nitrogen jet cutting pressure. Table 3 summarizes the traverse speed from which the charged UCNJ cuts the material through the whole thickness of the workpiece for mineral and vegetal abrasives.

Fig. 11 presents machined surfaces of flax/PLA composite obtained with UCNJ using abrasives in two configurations with a common traverse speed of the jet of V_a = 360 mm/min. Each configuration shows a low magnification at x70 (a and c) with its respective enlargement at x 400. Fig. 11 (a, b) was obtained using the vegetal walnut abrasives at a pressure of 200 MPa and an abrasive mass flow rate of 165 g/min. Fibers bundles, showing relatively short uncut fiber lengths, can be discerned with a gap at the fiber/matrix interfaces. Fig. 11 (c, d) shows the surface morphology of the machined surface generated by UCNJ using the garnet abrasives at a lower pressure (100 MPa) and the same traverse speed of 360 mm/min, and an abrasive mass flow rate of 200 g/min. Unfibrilated fibers and grooves are present on the machined surface along with crinkles on the workpiece beneath the flax fibers. Striations seem to only be visible for the walnut shell charged jet under these configurations.

4. Discussions

4.1. Pure nitrogen jet

The characteristics of the uncut-through kerf give access to the material removal rate that is the main wear characteristic. One of the parameters influencing the kerf depth is the jet traverse speed. When the jet meets the material, it encounters a surface that is almost parallel to the jet feed rate direction, maximizing hence the abrasive wear. As the jet moves upon the biocomposites, it encounters a surface that is orthogonal to its direction, changing thus the erosion wear from abrasion to impact wear. Besides, as the jet progresses into the biocomposites, it is confronted with the deflection from the material's kerf profile, combined with the displacement of the jet. Therefore, if the tap deflection is reduced, the abrasive wear is optimized enabling the material erosion. Hence, reducing the traverse speed increases the energy of the cut, leading to the increase of the kerf depth as water jets. However, the literature showed that lowering the material temperature contributes to an increase of its mechanical properties, which means that the machining would need higher energy. So how do those two contradictory phenomena interact within a UCNJ machining operation?

The second parameter of influence studied in this work on pure nitrogen cutting is the pressure of the jet. When it increases, it leads to a higher power of cut as shown in Equation (4), enhancing then the cutting energy. Besides, the jet can be seen as a beam of particles: when a particle impacts the material's surface, another will reach it, creating vibrations within the material. Those vibrations can be considered as loading and unloading cycles, which deteriorates the biocomposite at its interfaces, leading to a fatigue fracture. When the pressure increases, the strength of each loading/unloading cycle follows the same trend. Therefore, the pressure has two effects on the cutting process by increasing the speed as demonstrated from Equation (2) and thus the energy of the particles as well as the frequency of the particle/material interaction.

The data shown in Table 4 gives a comparison of the nitrogen jet's

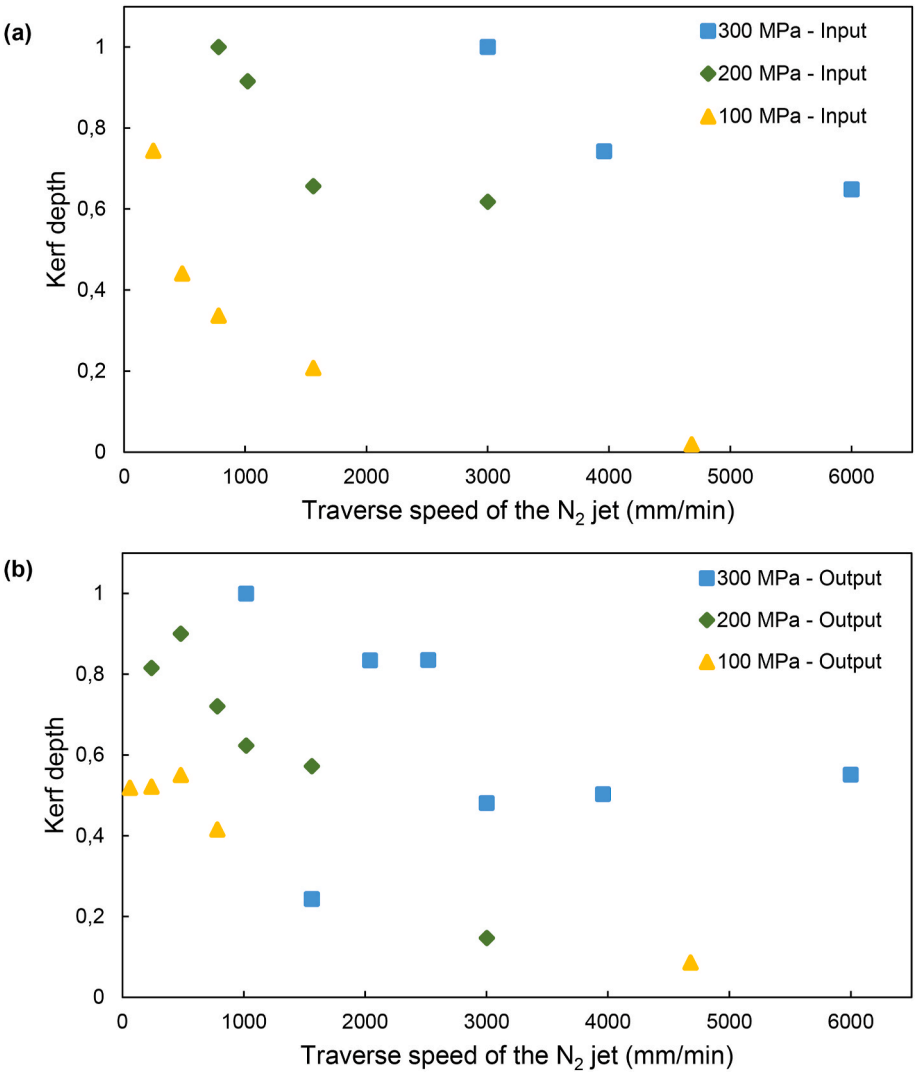

Fig. 7. Erosion rate of a flax/PLA biocomposite to an orthogonal cutting by the N_2 cryogenic fluid jet – (a) Input; (b) Output.

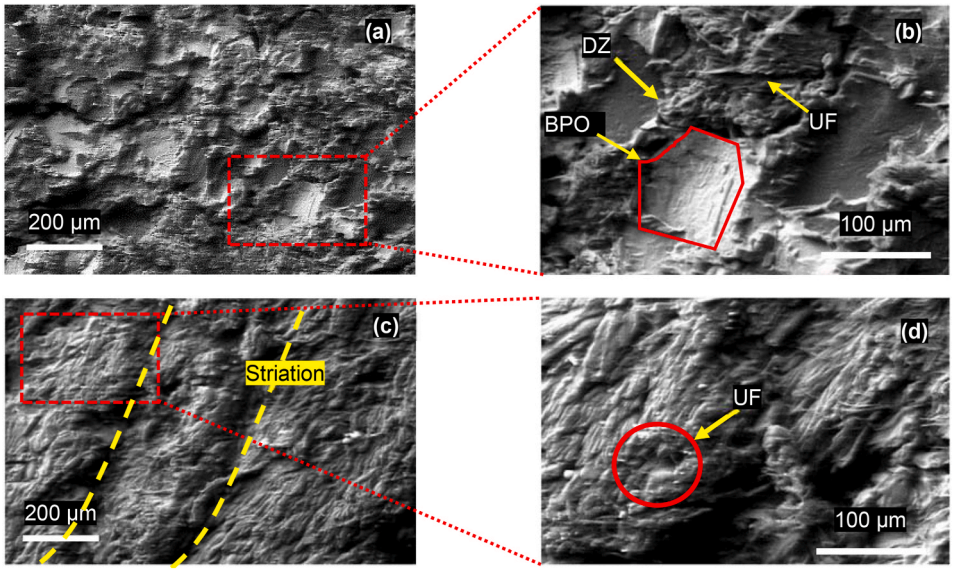

Fig. 8. SEM investigation of the effect of the pressure on the N_2 jet machining of a Flax/PLA biocomposites at (a, b) P = 200 MPa and V_t = 50 mm/min showing deformation zones (DZ) and brittle pulled out chips (BPC), (c, d) P = 300 MPa and V_t = 250 mm/min shows wide areas filled with uncut fibers (UF)).

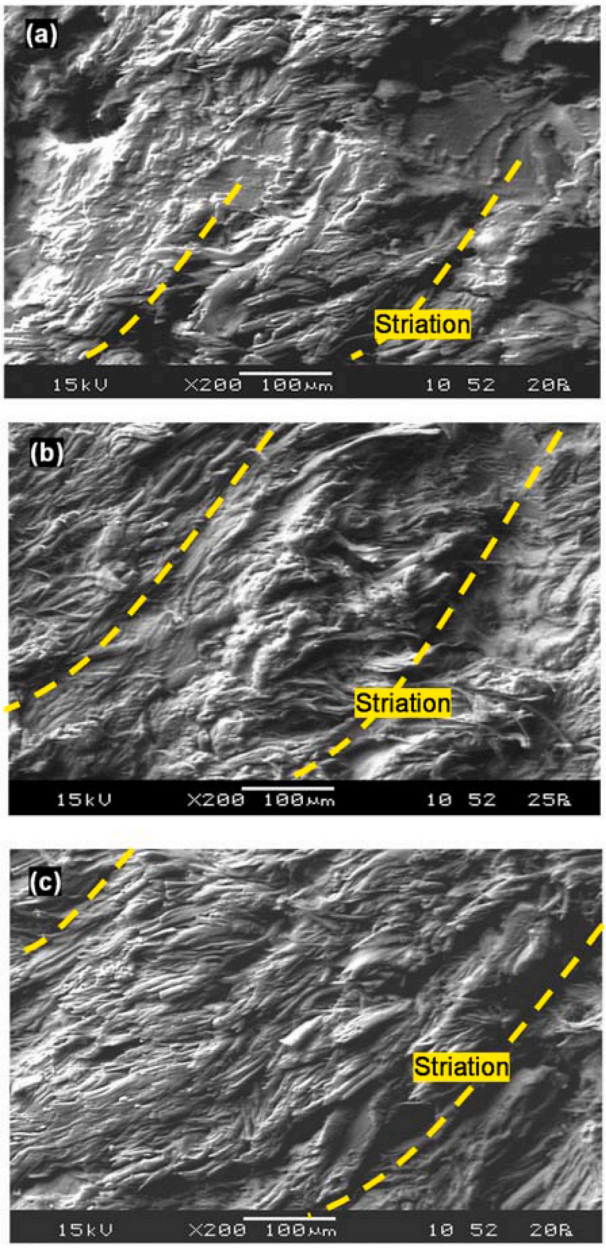

Fig. 9. SEM characterization of the machined profile of a Flax/PLA biocomposite cut with a pure CNJ at P = 300 MPa at three traverse speed: (a) 250 mm/min, (b) 500 mm/min, and (c) 750 mm/min.

speed calculated from Equation (2) at the pressure used in the experiments depending on the densities extracted from the NIST's models.

The slower the jet is, the more heat can be exchanged with its environment following Equation (1). Thus, the cooling of the material will be more effective at 100 MPa than at 300 MPa and this statement could explain the brittle pull-out and sharp edges noticed in Fig. 8 (a, b). These types of damages are a sign of brittle fracture mechanisms, indicating a brittle cutting regime. Although in the same picture, there seem to be deformed zones on the edges of the BPO containing a high density of uncut fibers which are, on the contrary, a sign of a ductile cutting regime. This type of machining demonstrates that complex mechanisms are involved and needs further investigation on the local interactions.

On the contrary, Fig. 8 (c, d) show that the jet was unable to cut the fibers and dissociated elementary fibers from the bundles instead. With high pressure under pure impact erosion wear with an angle of impact at 90° from the surface, the highly energetic eroding nitrogen particles hit the composites with mechanical energy and cryogenic temperatures from −175 °C to −150 °C. At that thermomechanical loading level, a strong gradient of temperature is developed within the composite preventing the whole material from cooling and applying thermal stresses. In this sense, when the speed of the jet is too high, natural fibers in the composite sample do not have the time to cool down to their brittle temperature. Moreover, the complex structure of cellulosic fibers enhances their insulating properties, increasing the gradient of temperature within the fibers compared to the matrix. Thus, the brittle cutting regimes could be induced within the matrix by the difference of heat conduction within the fibers and matrix.

To visualize the temperature effect, the exposure time of the material to the cryogenic temperature of the UCNJ can be calculated. The sapphire nozzle used had a diameter of 0.25 mm as defined in Table 2. If we consider that the jet has a diameter equal to the nozzle, the exposure time calculations of the material to the nitrogen are given in Table 5 as a function of the traverse jet speed. Thus, the cutting surface finish improves with the decrease in the traverse speed of the jet when other variables are held constant (see Fig. 9).

A dual effect of the convection exchanges of the cryogenic jet and the kinetic energy that depends on the exposure time can be deduced from Fig. 9. Indeed, the faster is the traverse speed of the N_2 Jet, the higher is the density and the length of uncut fibers. Both thermal and mechanical effects depend on the exposure time which can explain the trend of the erosion. Besides, the jet temperature is faraway below the ductile to brittle transition temperature of the machined biocomposite which is approximately about −45 °C for the PLA [8] and above −100 °C for flax fibers [9]. Thus, the nitrogen jet first interacts with the PLA matrix and then passes across the transverse direction of flax fiber bundles. As the temperature decreases into the material using conduction and convection, flax fibers rigidify from the large difference of temperature between the ambient temperature at 25 °C and the liquid nitrogen's temperature at −170 °C. When the flax fiber rigidifies, its mechanical properties are enhanced, leading to an increase in the cutting energy. Thus, the surface finish is improved with the decrease in the traverse speed of the jet when the other variables are held constant. By referring to the water jet cutting, this result is in line with the literature as one of the main parameters for water jet machining is indeed the traverse speed.

4.2. *Abrasive nitrogen jet*

For the analysis of the results from the abrasive test, the authors remind the reader of the garnet abrasives density ($\rho = 2.5$ g/cm^3) as well as the walnut shell abrasives density (ρ = 0.7–0.8 g/cm^3), which are even lighter than the fluid at the center of the jet (see Table 4). The cutting strength of those three materials depends on their kinetic energy which is related to their density. This can explain the cutting results summarized in Fig. 10. Walnut abrasives cut the biocomposite sample at the same pressure that the pure jet did with only a slight improvement on the traverse speed. The question here is: how could an abrasive nitrogen jet cut the biocomposite at a higher speed (360 mm/min compared to 50 mm/min for pure nitrogen jet) if the density of the walnut abrasive is lower than that of the nitrogen jet? Perhaps, as walnut abrasive particles are composed of polymeric materials, this vegetal abrasive densified within the jet stream before reaching the biocomposite, which enhances its cutting power. Another hypothesis is that walnut, being a hydrophilic material, has an adsorbed layer of gaseous water attached to its surface at ambient temperature. When the temperature decreases within the abrasive during the jet homogenization, this adsorbed water sublimates, creating small ice particles. These ice particles might be the ones enhancing the cut in this case. The abrasive UCNJ has completely achieved the cut of the sample only in one cutting condition with walnut abrasives, which is why we only noted one line on this type of abrasive. On the other hand, garnet abrasives showed substantial results by achieving the cut through the samples at a

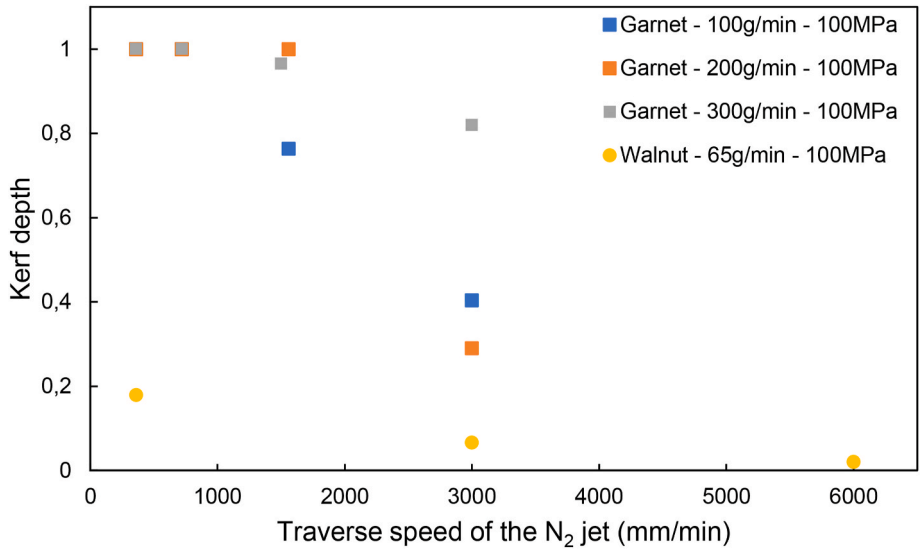

Fig. 10. Erosion rate of a PLA/Flax biocomposite by an abrasive cryogenic nitrogen jet using garnet or walnut as abrasives at different traverse speeds.

Table 3
Required traverse speeds to cut the biocomposite samples.

Pressure (MPa)	Abrasive Material	Sample Side	Abrasive Mass Flow rate (g/min)	Traverse speed (mm/min)
200	Walnut	/	165	360
100	Garnet	Input	100	720
			200	1560
			300	1560
		Output	100	720
			200	1560
			300	720

lower pressure (100 MPa) and low abrasive mass flow rates combined with high jet traverse speed (up to 1560 mm/min).

One particularity of Table 3 is the representation of the sample's sides from which the jet entered (input) and exited (output) the sample. This column is the mirror of the loss of energy of the jet within the material which is known to form striations on the material surfaces in abrasives water jet machining, impacting the depth of the kerf. Those striations can be noticed above a machining speed of 50 mm/min in pure UNCJ. However, it was not clearly noted for abrasive UNCJ.

In abrasive UCNJ cutting, the depth of cut increases depending on abrasives parameters such as the increase of abrasive mass flow rate and density, coupled to the high pressure of the jet and low traverse speeds. To compare with the pure jet, the use of abrasives enhances the cutting power of the jet by adding a new component to the kinetic energy as following: $E = E_{fj} + E_a$, where E is the total kinetic energy, E_{fj} is the kinetic energy of the jet, and E_a is the kinetic energy of the abrasives particles, which is similar to abrasive water jet cutting.

Walnut abrasives have indeed a low density (0.5–0.7 g/cm^3) and low hardness (3.5 Mohs). Walnut abrasives are hence rapidly accelerated within the nitrogen flow. At high speed, they are projected against the material's surface. Cryogenic temperatures in a range of {-175 °C to −150 °C} combined with the low hardness of the abrasive particles can enhance the occurrence of their fragmentation. Indeed, under the high orthogonal impact velocity on the machined surface, abrasive particles create multiple fragments of small size, hard enough to separate microfibrils but not to cut through the elementary flax fiber. After microfibrils separation, the following fragments would impact the cellulose microfibrils ending into the fibrillated elementary fibers.

A global observation from the SEM Fig. 11 can be made, unlike the first set of experiments; fiber bundles can be distinguished when using abrasives. From Fig. 11 (a) and Fig. 11 (c), abrasive particles seem to improve the tribological contact, obtaining smoother surfaces compared to the UCNJ machined surfaces shown in Fig. 8. Their use leads to reduce the length of the uncut fibers on the machined surface Fig. 11 (a) and Fig. 11 (c), compared to the results obtained under pure N2 jet machining Fig. 9 (a). To verify this hypothesis, further experiments need to be conducted to reach the same pressure and traverse speed magnitudes. To some extent, the addition of rigid abrasive particles may interfere with the angle of impact, improving the abrasion mechanism and thus the shearing of the fibers. Further observation can be made about the debris within the samples. It appears that very small fragments were found between the fibers particularly with high density under garnet abrasive particles. When directly looking at the sample (macroscopically) after the experiments, the machined surfaces showed shiny incrustations which indicate that the debris in abrasive nitrogen jet consists of fine powder. It appears that the fragmentation process is involved during abrasive cryogenic nitrogen jet (ACNJ) machining, especially at 300 MPa.

The nitrogen jet charged with garnet abrasives seems to enable much deeper cuts under a brittle cutting regime without any sign of fibrillation. The mineral abrasive provides higher mechanical energy during the impact due to its higher density (2.5 g/cm^3) and its higher hardness (7.5– 8.0 Mohs). Its thermal conductivity ($\lambda = 2.5$ W (m K)$^{-1}$) at ambient temperature [45] is also higher compared to that of PLA.

Therefore, the thermal exchanges with the abrasive jet could be stronger compared to the pure fluid nitrogen jet, and garnet abrasives can exchange more heat than walnut due to their nature. This rapid change of temperature helps the biomaterials to reach their DBTT, inducing a brittle rupture of the fiber. Nevertheless, as the jet proceeds into the thickness of the biocomposite, the jet's energy decreases, producing an erosion which is controlled by the density, hardness, and mass flow rate of the abrasives as well as its nature (mineral or vegetal).

5. Conclusions

This paper addresses the use of under-expanded nitrogen to form a cryogenic jet as a non-conventional cutting tool for developing advanced biocomposites machining process. When mixed with abrasive particles, this technique can improve the productivity of the process. Indeed, abrasive cryogenic N_2 fluid jet machining induces two wear phenomena composed of impact and abrasion wear. Under a pure cryogenic nitrogen jet, the loss of material by erosion is dominated by impact wear, whereas the erosion process is controlled simultaneously by abrasive and impact wear in the case of abrasive cryogenic nitrogen

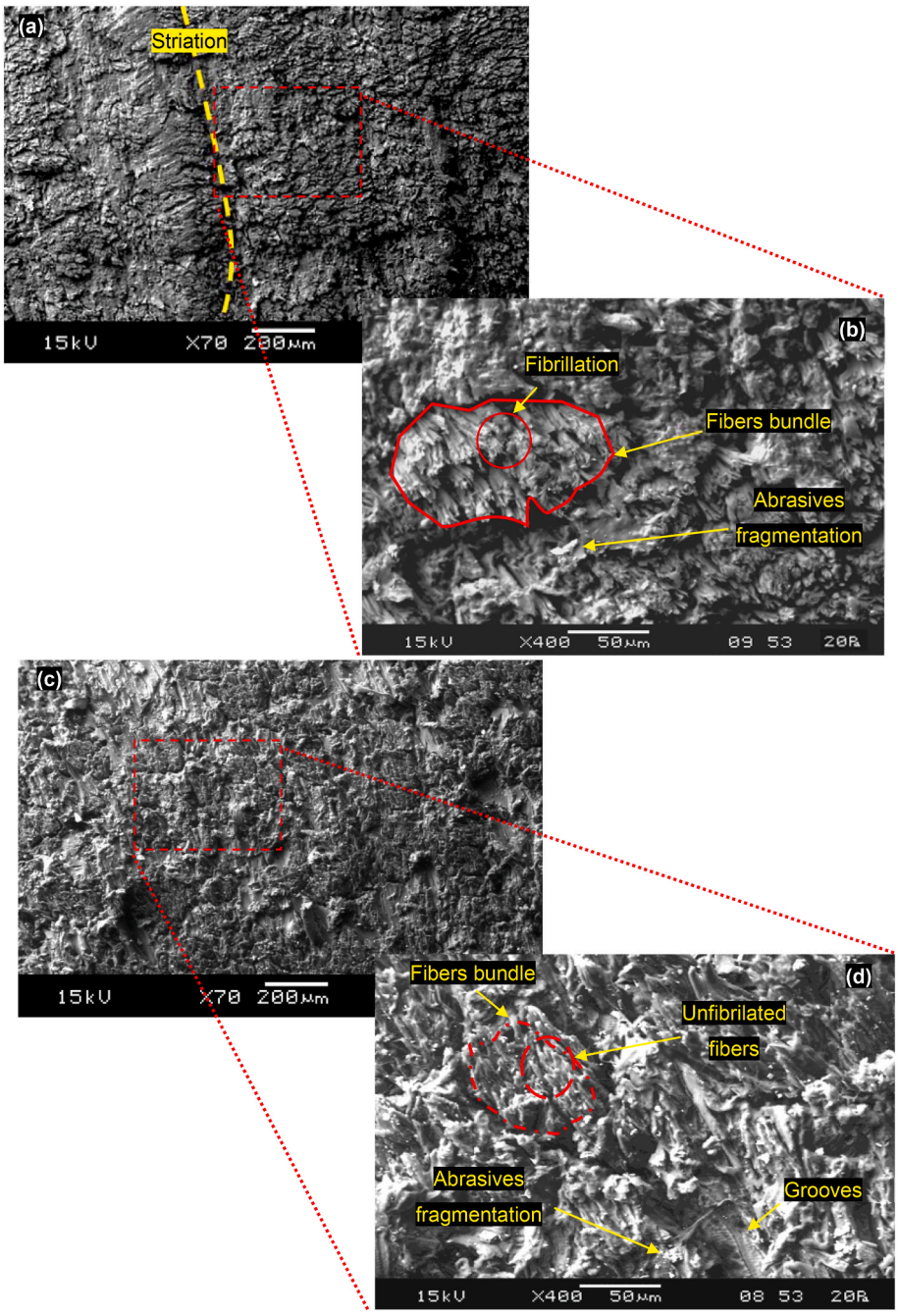

Fig. 11. SEM investigation of abrasive cryogenic nitrogen jet (ACNJ) for the following processing parameters: (a, b) $P_{N2} = 200$ MPa, $q_{walnut} = 165$ g/min, $V_a = 360$ mm/min; (c, d) $P_{N2} = 100$ MPa, $q_{garnet} = 200$ g/min, $V_a = 360$ mm/min.

Table 4
A comparison of the jet density and speed of cutting based on the jet pressure.

Pressure (MPa)	Density (kg/m^3)	Speed (m/s)
100	883	380
200	965	515
300	1007	617

Table 5
A comparison of the exposure time of pure nitrogen jet and the surface of bio-composite for different traverse speed values.

Traverse speed of the jet (mm/min)	Exposure time (s)
250	0.06
500	0.03
750	0.02

jet (ACNJ). Both the erosion rate and surface finish depend on the jet traverse speed, fluid jet pressure, and abrasive properties which corroborated the assumption that nitrogen jets and water jets share the same cutting behavior. However, thermal and mechanical impacts need better understanding. This study also introduces walnut abrasive as viable and sustainable abrasive particles for ACNJ. Investigation of the cutting power of bio-based abrasives should be made at higher pressures compared to conventional mineral abrasives to validate the use of this kind of abrasive for cutting applications. Optimal processing parameters and advanced wear studies will also be carried out with further instrumented experiments.

Declaration of competing interest

The authors declare that they have no known competing financial interests or personal relationships that could have appeared to influence the work reported in this paper.

Acknowledgments

This work was supported by the Région Grand-Est (France) and the CRITT-TJFU.

References

[1] A. Bourmaud, J. Mérotte, D. Siniscalco, M. Le Gall, V. Gager, A. Le Duigou, F. Pierre, K. Behlouli, O. Arnould, J. Beaugrand, C. Baley, Main criteria of sustainable natural fibre for efficient unidirectional biocomposites, Compos. Part Appl. Sci. Manuf. 124 (2019), https://doi.org/10.1016/j.compositesa.2019.105504, 105504.

[2] J. Ahmad, Machining of Polymer Composites, Springer US, Boston, MA, 2009, https://doi.org/10.1007/978-0-387-68619-6.

[3] J.E. Mark (Ed.), Physical Properties of Polymers Handbook, second ed., Springer, New York, 2006.

[4] K.J. Jem, B. Tan, The Development and Challenges of Poly (lactic acid) and Poly (glycolic acid), Adv. Ind. Eng. Polym. Res. (2020), https://doi.org/10.1016/j.aiepr.2020.01.002.

[5] K. Charlet, J.P. Jernot, S. Eve, M. Gomina, J. Bréard, Multi-scale morphological characterisation of flax: from the stem to the fibrils, Carbohydr. Polym. 82 (2010) 54–61, https://doi.org/10.1016/j.carbpol.2010.04.022.

[6] C. Poilâne, Z.E. Cherif, F. Richard, A. Vivet, B. Ben Doudou, J. Chen, Polymer reinforced by flax fibres as a viscoelastoplastic material, Compos. Struct. 112 (2014) 100–112, https://doi.org/10.1016/j.compstruct.2014.01.043.

[7] P.H.F. Pereira, M. de F. Rosa, M.O.H. Cioffi, K.C.C. de C. Benini, A.C. Milanese, H.J. C. Voorwald, D.R. Mulinari, Vegetal fibers in polymeric composites: a review, Polímeros. 25 (2015) 9–22, https://doi.org/10.1590/0104-1428.1722.

[8] M. Kaiser, H. Anuar, S. Razak, Ductile–brittle transition temperature of polylactic acid-based biocomposite, J. Thermoplast. Compos. Mater. 26 (2013) 216–226, https://doi.org/10.1177/0892705711420595.

[9] Thermal Insulation of Plastics, Technical Properties, (n.d.), https://omnexus.specialchem.com/polymer-properties/properties/thermal-insulation. (Accessed 12 August 2020).

[10] A Comparative Life Cycle Assessment of Building Insulation Products Made of Stone Wool, paper wool and flax, 2004, p. 14.

[11] A. Vinod, M.R. Sanjay, Renewable and sustainable biobased materials: an assessment on biofibers, biofilms, biopolymers and biocomposites, J. Clean. Prod. (2020), https://doi.org/10.1016/j.jclepro.2020.120978, 120978.

[12] A.R. Sanadi, D.F. Caulfield, Transcrystalline interphases in natural fiber-PP composites: effect of coupling agent, Compos. Interfac. 7 (2000) 31–43, https://doi.org/10.1163/156855400300183560.

[13] L. Ernst, Back, Lennart Salmén, Glass Transitions of Wood Components, Tappi J., 1982.

[14] V. Gager, A. Le Duigou, A. Bourmaud, F. Pierre, K. Behlouli, C. Baley, Understanding the effect of moisture variation on the hygromechanical properties of porosity-controlled nonwoven biocomposites, Polym. Test. 78 (2019), https://doi.org/10.1016/j.polymertesting.2019.105944, 105944.

[15] R. Teti, Machining of composite materials, CIRP Ann 51 (2002) 24, https://doi.org/10.1016/S0007-8506(07)61703-X.

[16] B. Bhushan, Introduction to Tribology, second ed., John Wiley & Sons Inc, Chichester, West Sussex, United Kingdom, 2013.

[17] A. Le Duigou, P. Davies, C. Baley, Exploring durability of interfaces in flax fibre/epoxy micro-composites, Compos. Part Appl. Sci. Manuf. 48 (2013) 121–128, https://doi.org/10.1016/j.compositesa.2013.01.010.

[18] A. Díaz-Álvarez, J. Díaz-Álvarez, J.L. Cantero, C. Santiuste, Analysis of orthogonal cutting of biocomposites, Compos. Struct. 234 (2020), https://doi.org/10.1016/j.compstruct.2019.111734, 111734.

[19] F. Chegdani, Z. Wang, M. El Mansori, S.T.S. Bukkapatnam, Multiscale tribo-mechanical analysis of natural fiber composites for manufacturing applications, Tribol. Int. 122 (2018) 143–150, https://doi.org/10.1016/j.triboint.2018.02.030.

[20] D. Wang, P.Y. Onawumi, S.O. Ismail, H.N. Dhakal, I. Popov, V.V. Silberschmidt, A. Roy, Machinability of natural-fibre-reinforced polymer composites: conventional vs ultrasonically-assisted machining, Compos. Part Appl. Sci. Manuf. 119 (2019) 188–195, https://doi.org/10.1016/j.compositesa.2019.01.028.

[21] F. Chegdani, B. Takabi, B.L. Tai, M.E. Mansori, S.T.S. Bukkapatnam, Thermal effects on tribological behavior in machining natural fiber composites, Procedia Manuf 26 (2018) 305–316, https://doi.org/10.1016/j.promfg.2018.07.039.

[22] H.N. Dhakal, S.O. Ismail, S.O. Ojo, M. Paggi, J.R. Smith, Abrasive water jet drilling of advanced sustainable bio-fibre-reinforced polymer/hybrid composites: a comprehensive analysis of machining-induced damage responses, Int. J. Adv. Manuf. Technol. 99 (2018) 2833–2847, https://doi.org/10.1007/s00170-018-2670-x.

[23] B. Vinod, L.J. Sudev, Investigation on effect of cryogenic temperature on mechanical behavior of jute and hemp fibers reinforced polymer composites, Appl. Mech. Mater. 895 (2019) 76–82. https://doi.org/10.4028/www.scientific.net/AMM.895.76.

[24] O. Yano, H. Yamaoka, Cryogenic properties of polymers, Prog. Polym. Sci. 20 (1995) 585–613, https://doi.org/10.1016/0079-6700(95)00003-X.

[25] S. Morkavuk, U. Köklü, M. Bağcı, L. Gemi, Cryogenic machining of carbon fiber reinforced plastic (CFRP) composites and the effects of cryogenic treatment on tensile properties: a comparative study, Compos. B Eng. 147 (2018) 1–11, https://doi.org/10.1016/j.compositesb.2018.04.024.

[26] M. Sprackling, Heat and Thermodynamics, Macmillan Education UK, London, 1993, https://doi.org/10.1007/978-1-349-12690-3.

[27] Y. Khalsi, F. Heim, J.T. Lee, A. Tazibt, N2 supercritical jet to modify the characteristics of polymer material surfaces: influence of the process parameters on the surface topography, Polym. Eng. Sci. 59 (2019) 616–624, https://doi.org/10.1002/pen.24977.

[28] A.W. Momber, R. Kovacevic, Principles of Abrasive Water Jet Machining, Springer London, London, 1998, https://doi.org/10.1007/978-1-4471-1572-4.

[29] P. Janković, T. Igić, D. Nikodijević, Process parameters effect on material removal mechanism and cut quality of abrasive water jet machining, Theor. Appl. Mech. 40 (2013) 277–291.

[30] A. Tazibt, F. Parsy, N. Abriak, Theoretical analysis of the particle acceleration process in abrasive water jet cutting, Comput. Mater. Sci. 5 (1996) 243–254, https://doi.org/10.1016/0927-0256(95)00075-5.

[31] M. Hashish, Pressure effects in abrasive-waterjet (AWJ) machining, J. Eng. Mater. Technol. 111 (1989) 221–228, https://doi.org/10.1115/1.3226458.

[32] F.L. Chen, J. Wang, E. Lemma, E. Siores, Striation formation mechanisms on the jet cutting surface, J. Mater. Process. Technol. 141 (2003) 213–218, https://doi.org/10.1016/S0924-0136(02)01120-2.

[33] A. Dhanawade, S. Kumar, Study on carbon epoxy composite surfaces machined by abrasive water jet machining, J. Compos. Mater. 53 (2019) 2909–2924, https://doi.org/10.1177/0021998318807278.

[34] S. Ferrendier, Influence de l'évolution granulométrique des abrasifs sur l'enlèvement de matière lors de la découpe par jet d'eau abrasif, Mécanique, Arts et Métiers ParisTech. https://pastel.archives-ouvertes.fr/tel-00005625, 2004. (Accessed 13 July 2020).

[35] A. Demirbas, Estimating of structural composition of wood and non-wood biomass samples, Energy Sources 27 (2005) 761–767, https://doi.org/10.1080/00908310490450971.

[36] G. Guerrero-Vaca, D. Carrizo-Tejero, Ó. Rodríguez-Alabanda, P.E. Romero, E. Molero, Experimental study for the stripping of PTFE coatings on Al-Mg substrates using dry abrasive materials, Materials 13 (2020) 799, https://doi.org/10.3390/ma13030799.

[37] Y. Yu, Q. An, Y. Zhou, S. Deng, Y. Miao, B. Zhao, L. Yang, Highly synergistic effects on ammonium removal by the co-system of Pseudomonas stutzeri XL-2 and modified walnut shell biochar, Bioresour. Technol. 280 (2019) 239–246, https://doi.org/10.1016/j.biortech.2019.02.037.

[38] H. Ventura, J. Claramunt, M.A. Rodríguez-Pérez, M. Ardanuy, Effects of hydrothermal aging on the water uptake and tensile properties of PHB/flax fabric biocomposites, Polym. Degrad. Stabil. 142 (2017) 129–138, https://doi.org/10.1016/j.polymdegradstab.2017.06.003.

[39] P. Shah, N. Khanna, Chetan, Comprehensive machining analysis to establish cryogenic LN2 and LCO2 as sustainable cooling and lubrication techniques, Tribol. Int. 148 (2020), https://doi.org/10.1016/j.triboint.2020.106314, 106314.

[40] F. Moggia, A. Benamane, T. Varet, V. Toulemonde, F. Richard, G. Anderson, F. Damerval, Nitrojet®: A Versatile Tool for Decontamination, in: A.Z. Phoenix (Ed.) vol. 11225, Cutting and Concrete Scabbling, 2011.

[41] Y. Hajji, D. Entemeyer, J. Serri, M. Yahiaoui, A. Tazibt, T. Grosdidier, High pressure cryogenic nitrogen jet for clean coating removal: experimental study of polyamide ablation, Mater. Sci. Forum. 941 MSF (2018) 1651–1655. https://doi.org/10.4028/www.scientific.net/MSF.941.1651.

[42] H. Laribou, C. Fressengeas, D. Entemeyer, V. Jeanclaude, R. Pesci, A. Tazibt, Effects of the impact of a low temperature nitrogen jet on metallic surfaces, Proc. R. Soc. Math. Phys. Eng. Sci. 468 (2012) 3601–3619, https://doi.org/10.1098/rspa.2012.0241.

[43] P. Dubs, M. Khalij, R. Benelmir, A. Tazibt, Contribution à la modélisation numérique de la détente d'un jet d'azote sous haute pression et basse température, 2009, p. 7.

[44] A. Regazzi, S. Corn, P. Ienny, J.-C. Bénézet, A. Bergeret, Reversible and irreversible changes in physical and mechanical properties of biocomposites during hydrothermal aging, Ind. Crop. Prod. 84 (2016) 358–365, https://doi.org/10.1016/j.indcrop.2016.01.052.

[45] N.P. Padture, P.G. Klemens, Low thermal conductivity in garnets, J. Am. Ceram. Soc. 80 (1997) 1018–1020, https://doi.org/10.1111/j.1151-2916.1997.tb02937.x.